13th World Conference on Earthquake Engineering
Vancouver, B.C., Canada
August 1-6, 2004
Paper No. 531

ANALYTICAL AND EXPERIMENTAL RESPONSE OF ASYMMETRIC STRUCTURES WITH FRICTION AND VISCOELASTIC DAMPERS

Juan C. DE LA LLERA[1], José L. ALMAZAN[2], Ignacio VIAL[3], Victor CEBALLOS[4], Marcos GARCIA[5]

SUMMARY

This article summarizes analytical and experimental results of linear asymmetric structures with frictional and viscoelastic dampers. Such energy dissipation devices may prove useful in controlling the uneven deformation demand occurring in structural members of torsionally unbalanced structures. Torsional balance is defined as a property of an asymmetric structure that leads to similar deformation demand in structural members equidistant from the geometric center of the building plan. It can be defined in a strong or a weak form. The latter, which allows for rotation of the building plan, only implies an equal norm of the displacement demand at resisting planes symmetric with respect to the geometric center. In general, it can be achieved by the use of energy dissipation devices by making the so-called empirical center of balance of the structure to lie on top of the geometric center. Shaking table results conducted on a mass and stiffness asymmetric six-story model with frictional dampers support the analytical results and the concept of weak torsional balance. Similar results may be extended to the use of viscoelastic dampers as well as for inelastic multistory asymmetric structures.

INTRODUCTION

The response of asymmetric structures during previous earthquakes has shown that the deformation demand may tend to concentrate in few resisting planes [1]. Consequently, design codes incorporate procedures to account for such irregular plan-wise displacement distribution, leading to different capacities among resisting planes. Instead of accounting for it, is it possible to balance the torsional response of an asymmetric structure?. The answer is affirmative and multiple alternatives may be implemented to do so. In this research, frictional and viscoelastic dampers are investigated and used to balance the torsional response of structures. Once lateral-torsional coupling is controlled in the structure, the problem transforms into that of a nominally symmetric structure, implying simpler design procedures, more efficient use of structural members, and more reliable structures.

[1] Associate Professor, Pontificia Universidad Católica de Chile
[2] Assistant Professor, Pontificia Universidad Católica de Chile
[3] Instructor Professor, Universidad de Los Andes, Chile.
[4] Graduate Student Researcher, Pontificia Universidad Católica de Chile
[5] Graduate Student Researcher, Pontificia Universidad Católica de Chile

In the study of torsional balance with energy dissipation devices (EDD), three aspects are of primary interest: (i) the optimal supplemental dissipation capacity selected for the design of the structure, (ii) the optimal plan location of dampers, and (iii) the response reduction factors achieved by the use of these optimal supplemental capacities and locations in plan. Of the three aspects, the second one will be emphasized herein. For simplicity in the presentation, the analysis is performed by considering the dynamic response of elastic single-story structural systems and a mass- and stiffness-asymmetric six-story experimental model. The interested reader may find further details of these results elsewhere [2,3,4].

Recent investigations have dealt with supplemental damping in asymmetric structures [e.g., 5]. It has been shown that in the case of viscous dampers, the reduction in response is highly dependent on the plan-wise distribution of the devices, implying that such reduction does not depend only on the damper eccentricity e_d but also on the radius of gyration of the supplemental damping ρ_d. By the appropriate use of viscous dampers, deformations demand in elastic and inelastic systems may be reduced up to three times [6]. Although not in the framework presented, the problem of the plan-wise distribution of supplemental dampers has also been considered earlier by minimizing different response quantities [7].

TORSIONAL BALANCE

Torsional balance is defined as a property of an asymmetric structure that leads to similar deformation demand in structural members equidistant from the geometric center (GC) of the building plan. It can be defined in a strong or a weak form. The former implies an uncoupling of the lateral and torsional motions and leads (nominally) to equal deformation demand in all structural members. The latter, which allows for rotation of the building plan, only implies an equal norm of the displacement demand at resisting planes symmetrically placed with respect to the GC. It is this weak form of torsional balance the one considered in this investigation. For the time being, it only matters the effect of torsional balance on the dynamic response of an asymmetric structure. The reader may find a detailed discussion of the idea of torsional balance with energy dissipation devices in Almazán [8].

For simplicity, a linear single-story model is considered to present the idea. The motion of its Center of Mass (CM) is defined by the two horizontal displacements u_x and u_y in the x- and y-directions, respectively, and a normalized rotation $l_x u_\theta$ about a vertical z-axis (Figure 1a). A single frictional damper is included along the Y-axis at a location e_d from the CM; the reason for not including ρ_d will become apparent later. The origin of the coordinate system is at the CM; plan dimensions are l_x and l_y in the X- and Y-directions, respectively. Next, we consider the case of e_{sy}=0.

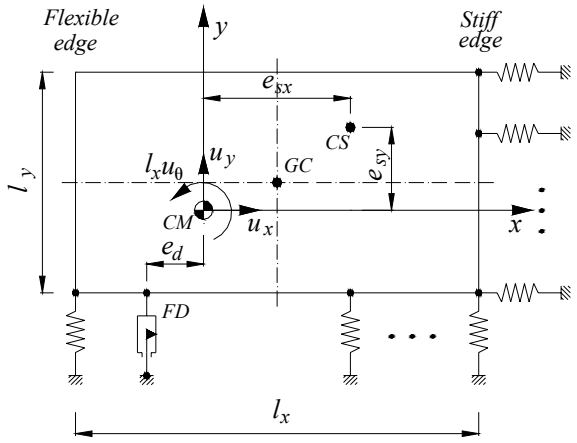

(a) General mass and stiffness asymmetric model

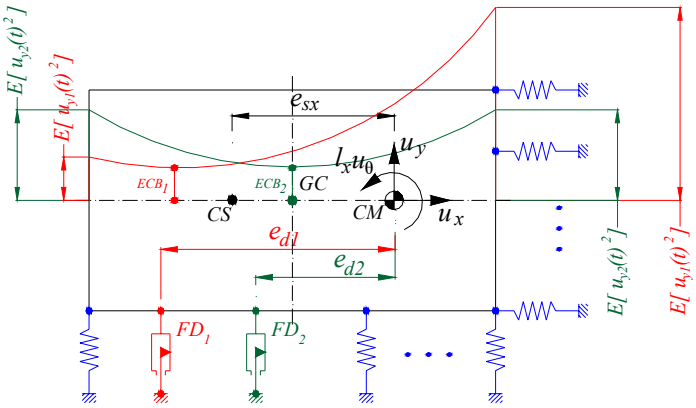

(b) Weak form of torsional balance

Figure 1. Structural system considered and weak torsional balance

Let us assume that the degrees of freedom $u(t)^T=[u_y(t,e_d)\ \ l_x u_\theta(t,\ e_d)]$ of the structure have been computed for a known location e_d of the frictional damper---for the sake of the analysis this is equivalent as if the motions at the CM had been instrumentally measured. The interesting point is to look at the correlation between the translation and rotation of the structure as the damper moves from one position to another. The displacement (velocity, and acceleration) at distance p from the CM would be of the form $u_y^{(p)}(t,\ e_d) = u_y\ (t,\ e_d) + p u_\theta(t,\ e_d)$ and, hence, the mean square value (MSV) of the displacement omitting the arguments t and e_d is

$$E\left[u_y{}^{(p)2}\right] = E\left[u_y{}^2\right] + 2pE\left[u_y u_\theta\right] + p^2 E\left[u_\theta{}^2\right] \tag{1}$$

This equation is quadratic in p (parabola), and for a given displacement profile of the building plan, the minimum value for $E[(u_y^{(p)})^2]$ is achieved at a point at distance p^* from the CM (Figure 1b), i.e.

$$p^* = -E\left[u_y u_\theta\right] / E\left[u_\theta{}^2\right] \tag{2}$$

It is easy to show that p^* also coincides with the point in plan such that the correlation between the displacement $u_y^{(p)}$ and rotation u_θ is zero [2]. Therefore, the point in the building plan for which there is zero correlation between lateral and torsional motions coincides with that of minimum MSV.

The point defined by the position p^* will be denoted, in the average sense presented (second moments or mean-square), as the Empirical Center of Balance (ECB) of the building plan. At the ECB, translations and rotations are statistically uncorrelated (orthogonal in the mean-square sense) and, hence, if the ECB and CM would coincide, the structure would behave, in the mean square sense, like an uncoupled system. Notice that if $p^* > 0$, the ECB is at the right of the CM and the correlation $E[u_y u_\theta]<0$; the opposite occurs for $p^* < 0$. Thus, the correlation between the lateral displacement and plan rotation changes in sign as the ECB shifts from one side to the other of the CM.

Moreover, the condition for torsional balance is that the ECB be at equal distance from both edges of the building plan [2]. This is a general result and it will be used throughout this study to express the optimal location of dampers. Results will also be compared with other heuristic rules presented elsewhere [6]. By using Equation (1) and substituting for displacement $\tilde{u}_y^*(t)$ and rotation $\tilde{u}_\theta^*(t)$ defined at the ECB, the MSV of the displacement at both edges of the building plan is

$$E\left[\tilde{u}_y^{(d)^2}\right] = E\left[\tilde{u}_y^{*2}\right] + d^2 E\left[\tilde{u}_\theta^{*2}\right] \tag{3}$$

A physical interpretation of Equation (3) says that because at the ECB the lateral and torsional motions are uncoupled in the mean-square-sense, the MSV of the displacements at the edges are a direct sum of the MSV of the lateral displacement at the ECB and the MSV of the rotation of the plan multiplied by the distance squared from the ECB to the edge of the plan. Furthermore, the MSV displacement values will be the same if and only if the distance d from the ECB to the edges is the same. Otherwise, the MSV of the displacement will always be larger at the edge farther from the ECB. By examining Equation (2), if the CM coincides with the GC, $p^*=0$; otherwise, p^* will be different from zero and equal to the distance between the GC and the CM.

Thus, the torsional balance condition with coincident CM and GC, i.e., $p^*=0$, represents an equation to find the damper eccentricity e_d such that it counteracts the effect of the stiffness eccentricity of the structure e_{sx} by forcing the ECB to lie on top of the CM and GC. Thus, the mirror optimal rule proposed earlier by Goel [6] has a conceptual justification in terms of the location of the ECB. However, it should be expected that for structures where rotation of the plan is more significant, say $\Omega_\theta \leq 1$, one could expect deviations with respect to the mirror rule. What is more interesting to note in the condition $p^*=0$ is that it only states the location of the vertex of the parabola of Equation (1), which is the ECB, leading to equal MSV of displacements at points equidistant from the GC and the weak torsional balance (Figure 1b). We could control further the curvature of such parabola by placing additional dampers away and symmetrically from the GC (ECB). This will move the design toward the direction of strong torsional balance.

The ECB is not in general a center of stiffness, damping, or strength. Its location depends on the same parameters as the response of the structure does and $p^*=0$ states a general condition we need to satisfy to achieve weak torsional balance in the structure but it does not say explicitly how to achieve it. The latter depends primarily on the stiffness, damping properties, and location of the damper as well as the dynamic properties of the structure. Because of the nonlinear nature of the problem, the optimal location of the damper e_d needs to be computed by any algorithm to find roots of a nonlinear equation.

In the previous derivations we have not used any assumption on the response of the system, and considered $u_y(t)$ and $u_\theta(t)$ as available signals coming from an elastic or inelastic, single or multistory structure, with or without dampers. Therefore, the concept of the ECB is completely general, and includes, for instance, the behavior of any inelastic structure with any type of damper subjected to any ground motion. Shown in Figure 2 is the inelastic earthquake response of a structure with 3 resisting planes in the Y-direction and uncoupled torsional-to-lateral frequency ratio Ω_θ=1.25 subjected to the Sylmar earthquake. The structure is defined by lateral frequency ratio Ω_x=1, normalized static eccentricity e_{sx}=0.08, uncoupled lateral period T_y=1s, and plan ratio α=0.5. Each plane is modeled considering three inelastic Bouc-Wen elements in the Y-direction representing a steel structure with a total normalized capacity F_{dy}=0.3. The initial stiffnesses of the resisting planes k_{oy} were selected proportional to their capacities. Moreover, the frictional damper selected had a normalized capacity F_{dy}=5%, initial stiffness k_o, ten times that of the structure, and Bouc-Wen parameters A_o=1, β=γ=0.5, n=10 and κ=0. As it is shown in the figure, the structure without a frictional damper shows inelastic displacement offsets of the flexible edge and significant discrepancies between the peak displacements at the stiff and flexible edges of the structure. For this case, the correlation between lateral and torsional motions is $\rho_{y\theta}$=-0.52. By placing the damper on the flexible edge, the correlation decreases to $\rho_{y\theta}$=0.361, but large discrepancies are observed between the displacement histories at both edges of the plan. Finally, by placing the frictional damper at the optimal value e_d^*= -0.17l_x, the correlation is reduced essentially to zero, the MSV of the displacements at both edges are identical, and the peak responses are quite similar.

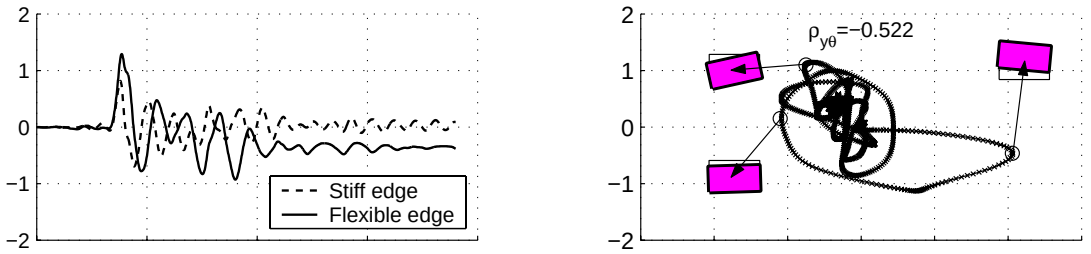

(a) Structure without FD.

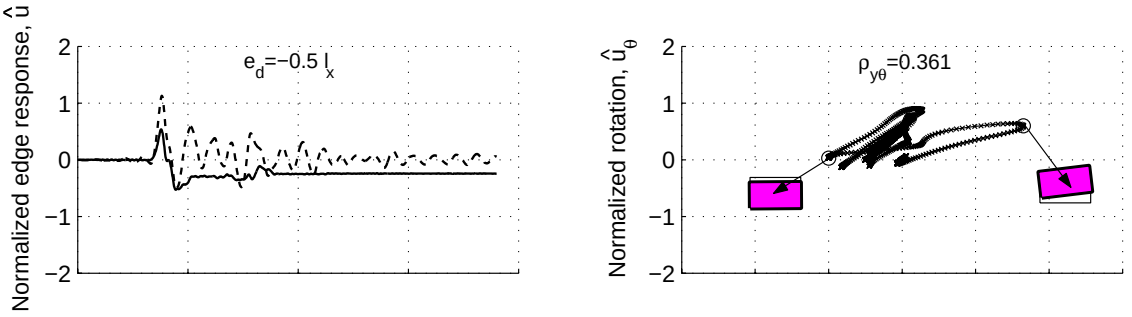

(b) FD at flexible edge.

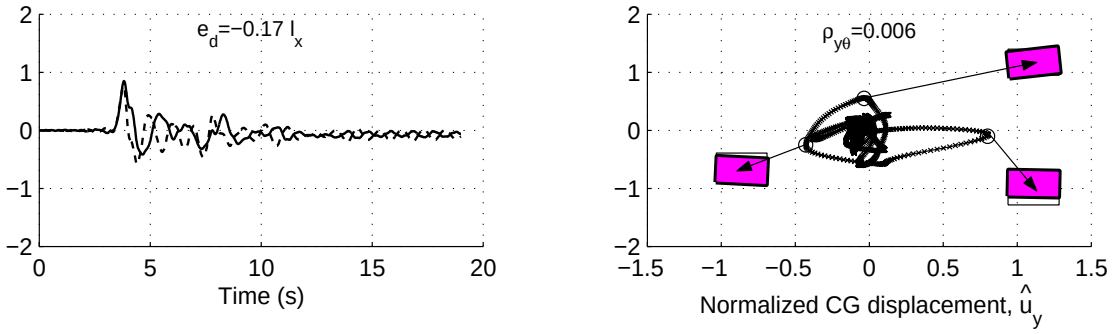

(c) FD at optimal location.

Figure 2. Typical inelastic response of a torsionally stiff asymmetric structure (Ω_θ=1.25, e_{sx}/l_x= 0.08) with and without an FD placed at the flexible edge and at the optimal location

The results shown in Figure 3 for inelastic structures with Ω_θ=1 and 1.25 validate the general idea of the ECB presented in this section. Thus, the analysis shows that the optimal damper eccentricities are for these structures e_d^* = -0.03l_x and -0.17l_x, respectively. These eccentricities are such that place the ECB on top of the CM of the structure. For this damper location, the standard deviations of the response at the stiff and flexible edges are the same and the correlation between lateral and torsional motions are zero. Thus, the condition imposed by $p^*=0$ is still valid for this inelastic case. The same would happen if we select the motions of an arbitrary inelastic multistory structure, showing that the stated condition to define torsional balance (but not the value) remains invariant with the structure that generates the response.

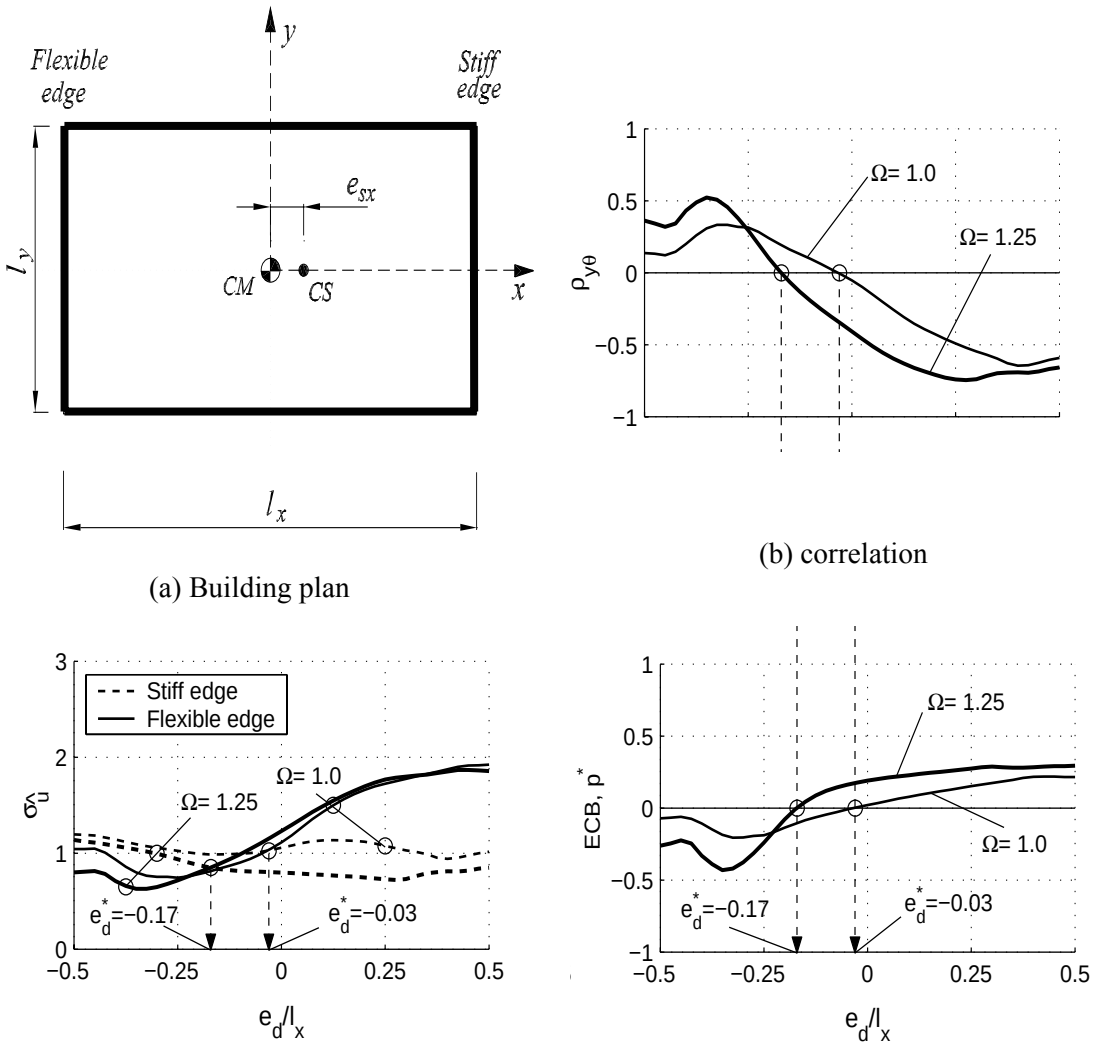

(a) Building plan

(b) correlation

(c) stiff and flexible edge response

(d) empirical center of balance

Figure 3. Cross-correlation between the elastic lateral and rotational motion, standard deviation of the stiff and flexible edge response, and empirical center of balance (ECB) for a torsionally flexible (Ω_θ=1.0) and stiff (Ω_θ=1.25) structure.

ANALYTICAL RESULTS

In this investigation, 3 artificial subduction type earthquake records compatible with the design spectrum of the Chilean code for seismic isolation and 5 impulsive ground motions were considered. The artificial motions correspond to a design spectrum with 10% probability of exceedance in 50 years and stiff soil condition (shear wave velocity 400 m/s < V_s <900 m/s); the impulsive earthquake records are Arleta, Sylmar, Newhall (1994), Corralitos (1989), and Kobe (1995).

As an example, consider the earthquake response of structures with frictional dampers (FD) subjected to the impulsive ground motions. Optimal average damper eccentricities for the five impulsive ground motions are presented in Figure 4 as a function of the normalized eccentricity e_{sx}, three values of the torsional-to-lateral frequency ratio Ω_θ = 0.8, 1, and 1.2, three uncoupled structural periods periods T_y =

0.5,1, and 2s, and three frictional damper capacities β = 5%, 10%, and 20%. The optimal values presented for e_d* correspond to average values obtained for the five records and are associated with the optimal torsional balance criteria (p*=*0*). Stiffness eccentricities e_{sx} vary from 0 to 0.25. The trends observed in e_d* are similar to those obtained for subduction type motions; naturally, there exists values of e_{sx} for which certain singularities in the response are observed. In general, as the static eccentricity e_{sx} increases, the optimal eccentricity of the damper also increases but to the opposite side with respect to the CM. This is consistent with the trend inferred by the mirror rule [6]. It is apparent that for the shorter structural periods $T_y \leq$ 1s, torsionally flexible structures Ω_θ = 0.8, and small static eccentricity values, say $e_{sx} < 0.05$, the optimal location of the damper is on the same side as the static eccentricity of the system. In those cases the mirror rule would fail to predict the right location of the damper. Also, as the structure becomes more flexible, a very simple rule would be to locate the damper close to the CM of the structure. Besides, as the capacity of the dampers increase, the slopes of the optimal eccentricity curves decrease. Thus, a heuristic criteria for optimal damper location should include the damper capacity as a parameter. This is consistent with the physical intuition that shows that for larger capacities, small variations in the damper location enable us to torsionally balance, at least in the weak sense, the building plan. On the other hand, torsionally stiffer structures require larger frictional capacities to balance the plan and, hence, optimal damper eccentricities are also a function of the period of the structure and the torsional-to-lateral frequency ratio. Results for subduction type ground motions may be found elsewhere [2].

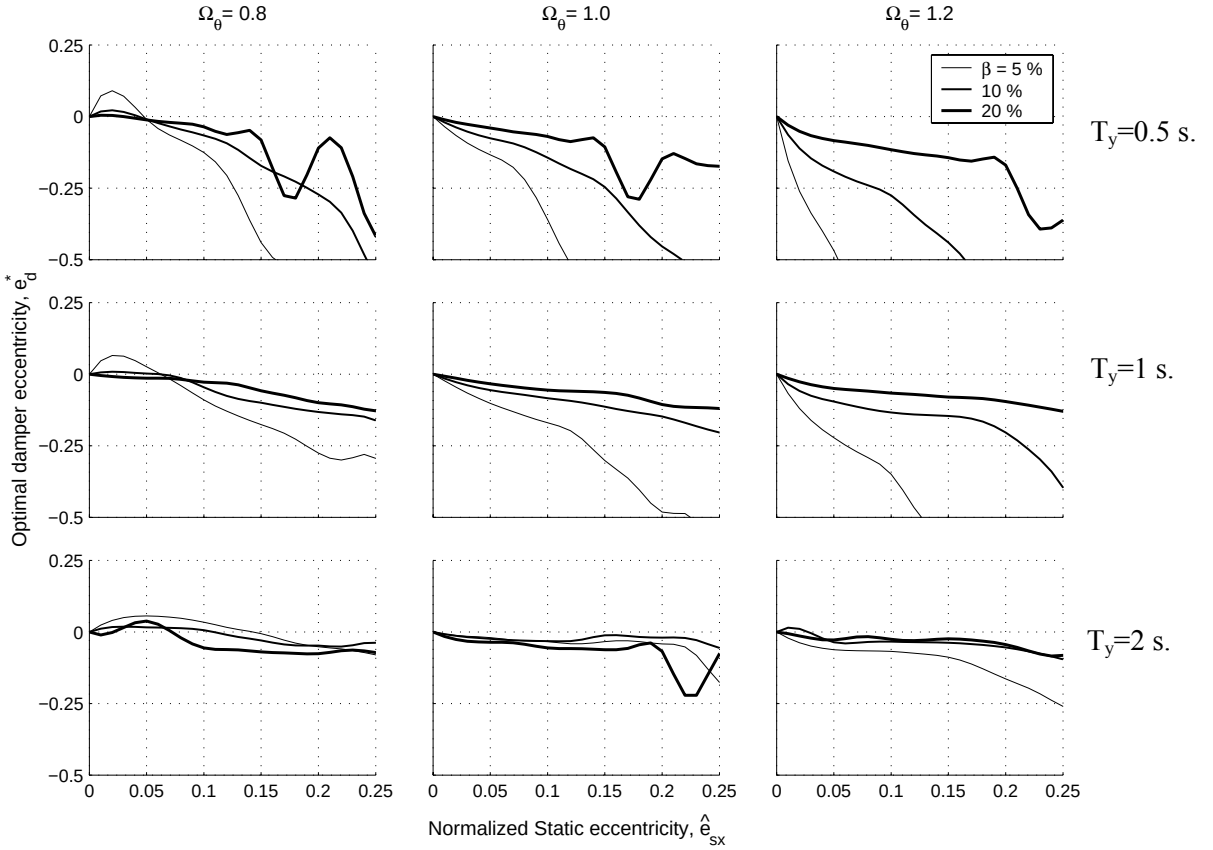

Figure 4. Mean results of the optimal FD location for impulsive type ground motions as a function of normalized static eccentricity for Ω_θ= 0.8, 1.0, 1.2 and lateral period T_y= 0.5, 1.0 and 2.0 s.

Shown in Figure 5 is a comparison between the normalized edge displacements, reduction factors, and torsional index as computed from the optimal balance and mirror rule for structures with uncoupled lateral period T_y = 1s. In the figure, the average values of e_d* obtained for all records are used to compute

the responses presented. Results for frictional capacity F_{yd} = 5% and 20% and two uncoupled torsional-to-lateral frequency ratios Ω_θ = 0.8 and 1.2 are considered. The first row of plots shows the stiff and flexible normalized edge displacements, the second row shows the torsional index, defined as the ratio between the maximum absolute difference between the lateral displacements at the flexible and stiff edges over the displacement at the CM of the same structure, and the third row, the displacement reduction factors at both edges $\hat{u}_f$ and $\hat{u}_r$. For static eccentricities $e_{sx} < 0.20$, the peak displacements at both edges computed with the optimal criteria are similar. The discrepancies observed in their mean values are due to the variability in response caused by the different ground motions. For this range of eccentricities, torsional amplifications relative to the symmetric case are less than 40% and reduction factors relative to the asymmetric response of the structure without dampers range between, say, 2 and 0.7. Therefore, though in most cases the use of frictional dampers leads to response reduction factors larger than 1, there exists cases, such as for Ω_θ = 1.2 and $\beta = 0.05$, where the amplifications of the stiff edge may be slightly larger than for the structure without dampers. However, reduction factors are misleading since the lateral displacement at the building edges of the structure with dampers is still more balanced than the response of the original asymmetric structure without dampers. Although, in general, normalized edge displacements computed with the optimal criteria present smaller discrepancies than those obtained with the mirror criteria, both lead to similar results. Finally, torsional indices increase with static eccentricity and reach stable values of about 2 to 4 for $e_{sx} > 0.1$. Results for other structures as well as for other damper capacities follow similar trends [2].

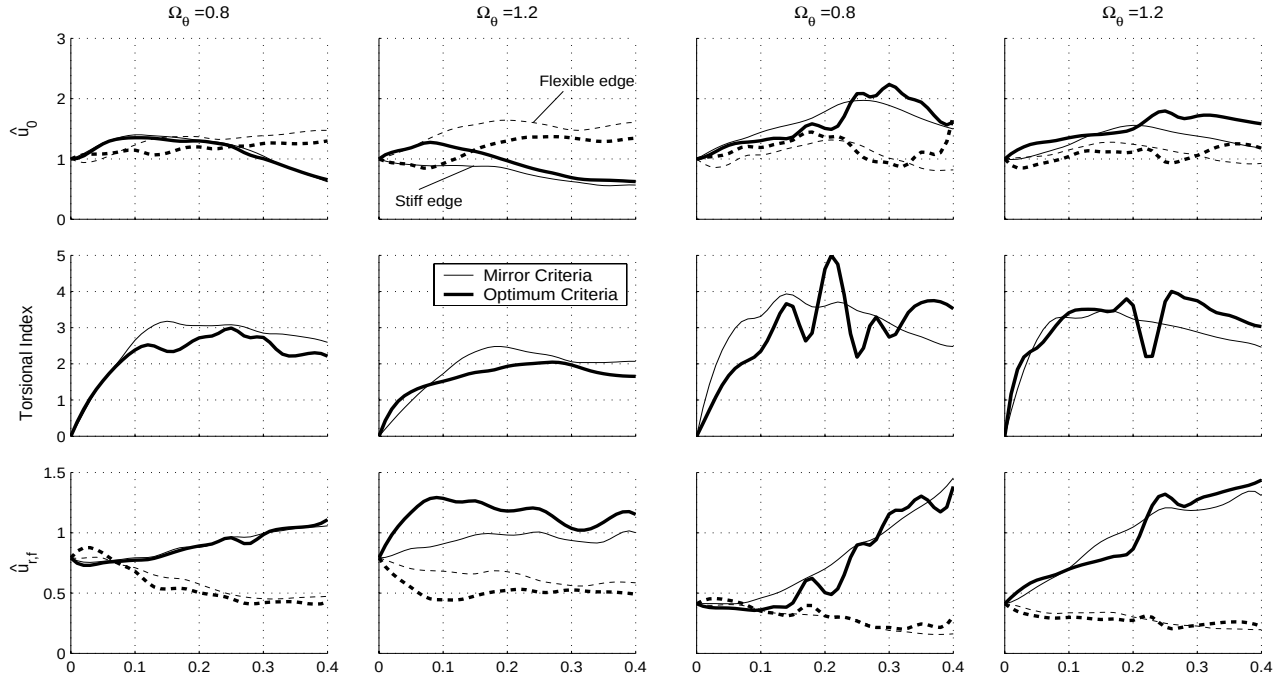

Figure 5. Comparison of normalized displacement, torsional index, and displacement reduction factors for T_y=1.0 s with FD capacities 5% and 20%, subjected to impulsive ground motions.

Let us extend the analysis to the case of an asymmetric structure with a viscoelastic damper modeled as a Maxwell and Kelvin element in parallel. The constitutive properties of the damper are calibrated with an experimental Scotchdamp compound. The storage and loss moduli for the dampers are represented by the expressions $S(\omega)=\alpha_g G'(\omega)$ and $L(\omega)=\alpha_g G''(\omega)$, where $\alpha_g = A_c n_c / t_r$ represents the geometric factor for the damper relating the shear area $A_c n_c$ with the layer thickness t_r. These damper design parameters are reflected in two global structural parameters, the damper-to-structure stiffness ratio $\Omega_s(\omega)$ and the

supplemental damping $\xi_s(\omega)$. Assuming that the loss factor $\eta(\omega) = L(\omega)/2S(\omega)$ is known for a viscoelastic damper, there exists a relationship between $\Omega_s(\omega)$ and $\xi_s(\omega)$. Consequently, results will be presented for combinations of these two parameters, which values will be defined at the uncoupled lateral frequency of the structure ω_y.

Similar analytical results of optimal damper location as those presented earlier in Figure 4 are shown in Figure 6 for viscoelastic dampers and structures subjected to the Sylmar record (Northridge 1994). Three uncoupled structural periods T_y = 0.5, 1, and 2 s and uncoupled torsional-to-lateral frequency ratios Ω_θ= 0.8, 1, and 1.2 are considered. Besides, a wide range of normalized structural static eccentricities e_{sx} = 0-0.25 was considered. Although the details of these curves and those of Figure 4 may be different, the results follow similar general trends.

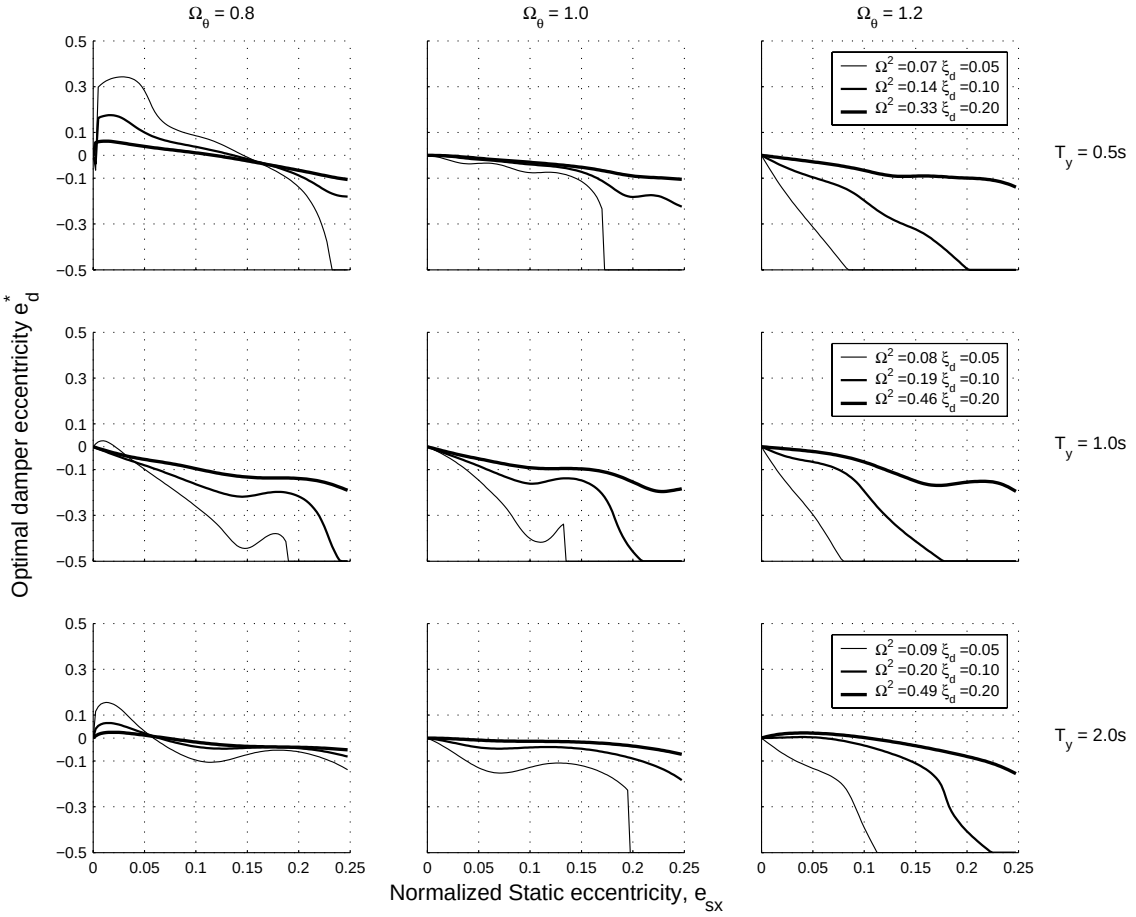

Figure 6. Optimal viscoelastic damper location for Sylmar ground motion as a function of normalized static eccentricity for Ω_θ= 0.8, 1.0, 1.2 and uncoupled lateral period, T_y= 0.5, 1.0 and 2.0 s.

For instance, for torsionally flexible structures ($\Omega_\theta < 1$) and static eccentricities $e_{sx} < 0.05$, the damper should be placed on the same side as the positive eccentricity. As the torsional stiffness of the structures increases ($\Omega_\theta > 1$), the relationship between the optimal damper eccentricity e_d and the static eccentricity e_{sx} becomes more closely linear and the mirror rule [6] is conceptually justified. However, as it was expected, the optimal eccentricity values are dependent on the damper capacity; for a given static eccentricity, smaller capacities require larger damper eccentricity values to counteract for e_{sx}, especially for torsionally stiff structures. It is also apparent that for several structural eccentricities is not possible to

achieve the weak torsional balance with the capacities defined for the viscoelastic dampers. As a general rule for $e_{sx} > 0.05$, optimal damper eccentricities tend to increase with an increase in e_{sx} but with opposite sign. Such increase depends on Ω_θ, $\hat{e}_s$, and the damper stiffness ($\Omega_s(\omega)$) and dissipation capacity $\xi_s(\omega)$. Additional results with viscoelastic dampers may be found elsewhere [4].

EXPERIMENTAL RESULTS

The structural model used in this study is a 6-story frame building with square plan and one bay of span length 860 mm (Figure 7), uniform story height h = 500 mm, and total building height H = 3000 mm. The model was built in duralumin in a geometric scale E_L = 1/7. To mantain an acceleration scale E_A equal to 1, time had to be scaled down in the model by a factor of $\sqrt{7}$. Hollowed beams and columns with square box-shapes of sides 30 mm and 40 mm, respectively, and 1.5mm thickness, are used in the model. To enforce rigidity in the beam-column connections, a perforated steel core was introduced inside the beams and columns and it was bolted to L-shaped stiffeners placed at the bottom and top faces of the beam. Prestressed steel cables of variable diameter (ϕ=1.5, 2, and 3 mm) were used to brace laterally the flexible structure. The floor diaphragm is a square steel plate of side 820 mm with a square central orifice of side 410 mm, plate thickness t=50mm, and total weight of the structural model W_T =7180 N. In order to achieve different torsional-to-lateral frequency ratios in the model, horizontal arms of length l_a= 2800 mm were fixed to the structure at each floor level (Figure 7). To achieve different mass eccentricities, additional weights w_m = 250 N were fixed on these arms at variable distances from the CM.

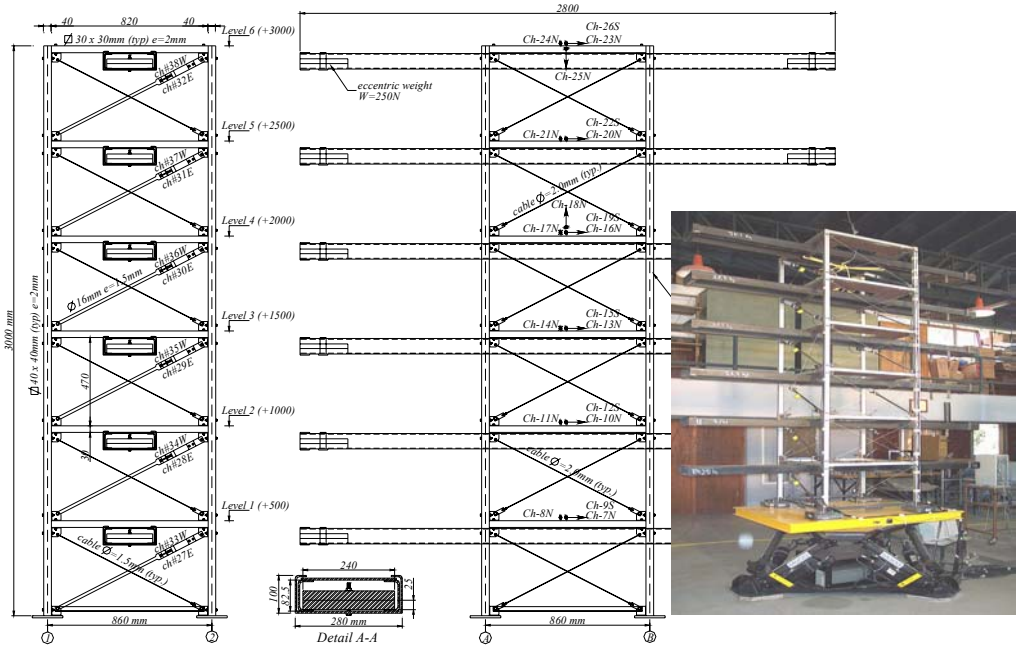

Figure 7. Six-story building model and sensors location.

The model was instrumented with 26 acceleration channels to measure floor accelerations and 12 displacement channels to measure the FD deformations. Six accelerometers were placed on the moving platform to measure the input motions, 18 were place in horizontal triplets at each floor to measure the lateral accelerations, and 2 were placed to measure vertical accelerations on the 4th and 6th floors. The 12 displacement potentiometers were placed diagonally in pairs along resisting planes A and B. The layout of sensors enables us to compute all floor accelerations in the two principal directions of the structure and the rotational motion of each floor relative to a vertical axis; it also enable us to evaluate directly the story

drifts and the displacements of each FD in the structure. Moreover, accelerations are used to calculate story shears and torques as well as response modification factors due to lateral-torsional coupling.

The experimental investigation assumed six different structural configurations. The first three considered the earthquake behavior of: (i) a nominally symmetric building (M_1); and (ii) mass eccentric building configurations (M_2, M_3), both with FD along planes 1 and 2 (Figure 8a).

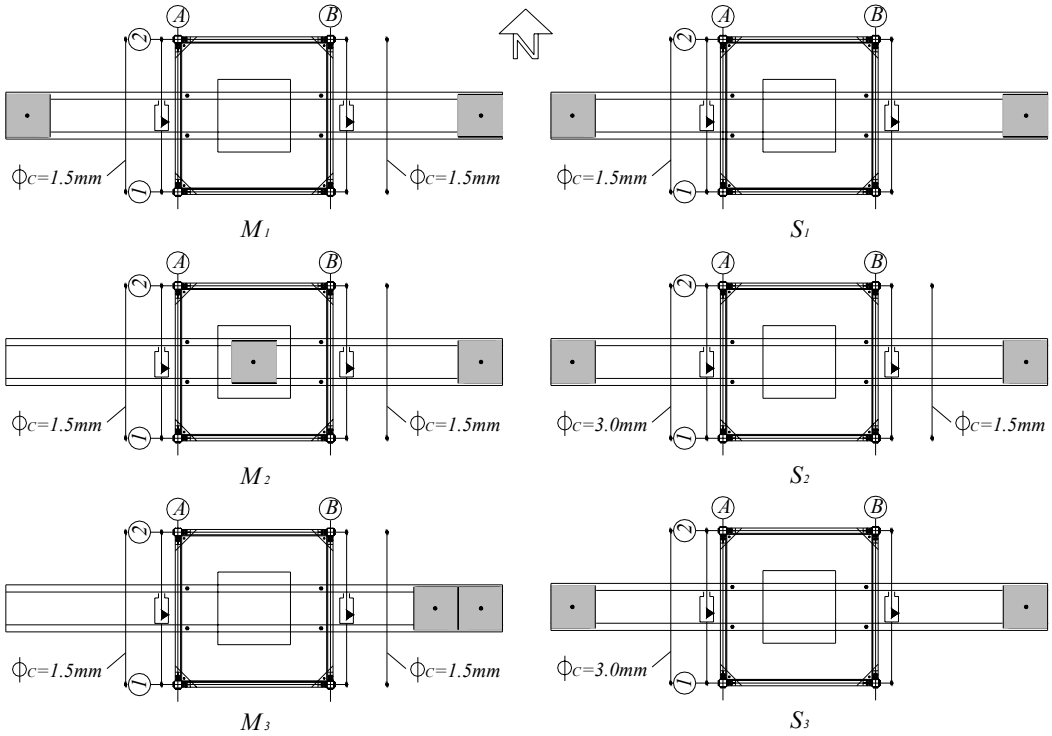

(a) Mass eccentric configurations (b) Stiffness eccentric configurations

Figure 8. Experimental models considered in the analyses.

All mass eccentric configurations include two prestressed cable diagonals of diameter ϕ=2mm along resisting planes 1 and 2, and a single prestressed diagonal of diameter ϕ=1.5mm along resisting planes A and B. The extra weights were selected in order to have a nominal frequency ratio range from Ω=0.9 to 1.2. Because of the time scale $E_T = \sqrt{7}$, the structural model represents actual buildings with periods varying from 0.7s to 1.1s, approximately. The second phase considered three different stiffness asymmetric configurations with and without frictional dampers. The configurations considered are presented in Figure 8b. All stiffness eccentric configurations are mass symmetric and include either prestressed cable diagonals of diameter ϕ=1.5 or 3mm along resisting planes *A* and *B*. Frictional dampers are double teflon-steel sliders with calibrated compression springs to control sliding capacities [3]; minimum and maximum frictional coefficients vary from 5.9% to 15.5%, respectively.

Scaled-down three-component earthquake records that include near-field ground motions as well as far-field subduction type ground motions were considered: 20% of Newhall (Northridge, 1994; PGA=0.59g), 30% of El Centro (Imperial Valley, 1940; PGA=0.31g) and 30% of Melipilla (Chile, 1985; PGA=0.69g). For the sake of brevity, only the results for the Newhall record will be presented herein.
The responses next correspond to standard deviations of measured rotations and edge and CM displacements. Moreover, "type-Ξ" responses, which represent a quotient between the peak displacement response due only to plan rotation and translation measured at the CM, are also computed. Finally, the

square root of the sum of the variances of the normalized degrees of freedom u_x and $l_x u_\theta$ for each floor is also considered.

Shown in Figures 9 and 10 is the dynamic response of the fourth-floor for the stiffness and mass eccentric configurations and the different damper locations.

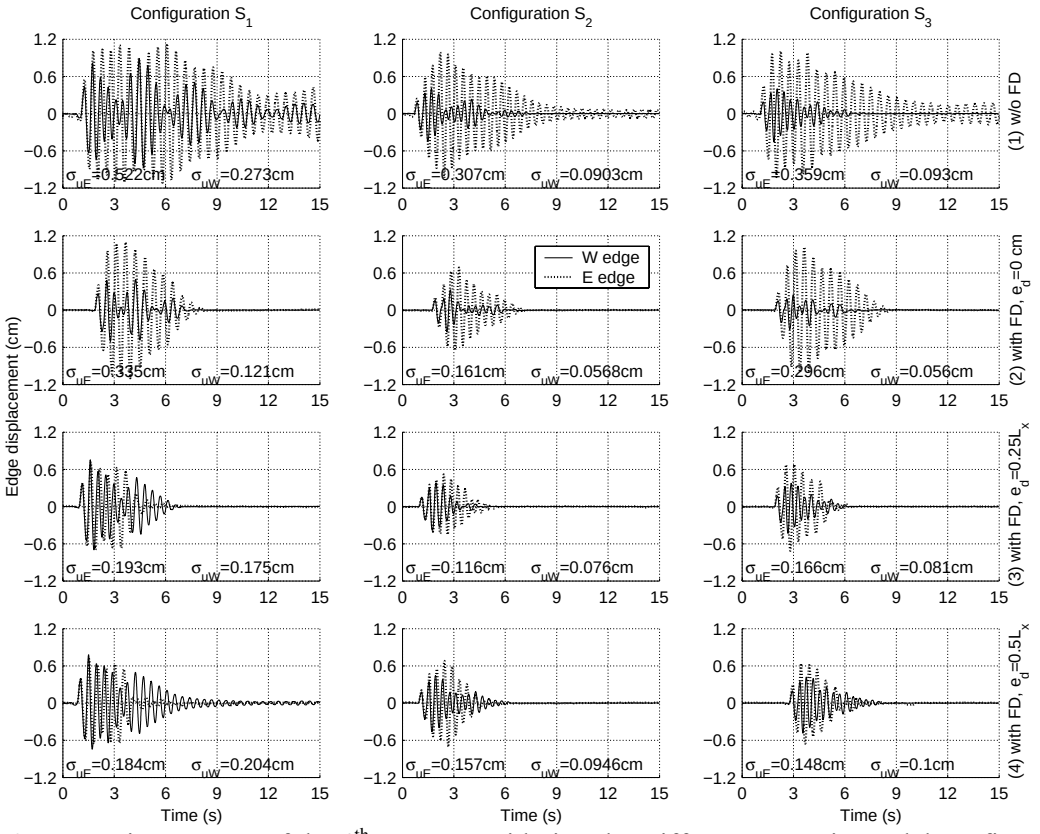

Figure 9. Dynamic response of the 4th-story, considering the stiffness eccentric model configurations.

It is apparent from the figure that frictional dampers considerably reduce the dynamic response of the structure. More important, they change the relative values of the response at both edges and, hence, prove that it is possible to modify the response of the asymmetric elastic structure by the simple incorporation of friction. By realizing that less than 5.2% of the weight of the structure is applied as a friction capacity in this model, this simple observation justifies the use of these devices to achieve torsional balance. Another known but interesting observation is that the damper location has an important effect on the relative deformations of both edges. Notice at the bottom of each plot the standard deviation of the displacement at the East and West edge. By comparing these values for configurations S_1, S_2, and S_3, the closest standard deviations are achieved in each model for e_d between $0.25l_x$ and $0.5l_x$.; a similar comparison with mass eccentric systems M_1, M_2, and M_3 (Figure 10) shows that with the capacities selected we are not able to balance the standard deviation of edge displacements and the best responses are achieved for maximum $e_d = 0.5l_x$. Also notice that in spite of the nominal symmetry of the structure, edge responses are still quite different for the symmetric configuration M_1 as a result of several accidental factors. Finally, response reduction factors due to the FD range between 2 and 3 for this earthquake.

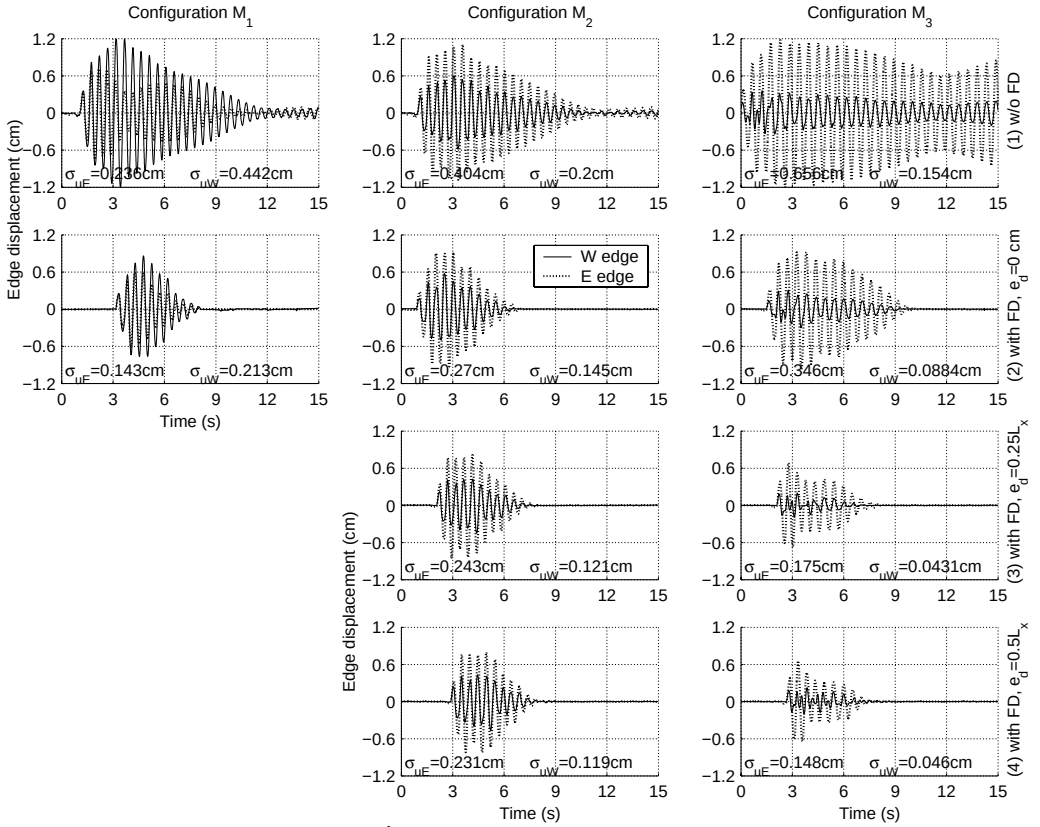

Figure 10. Dynamic response of the 4th-story, considering the mass eccentric model configurations.

Relevant information about the optimal location of the ECB in these structures may be better understood by examining Figure 11. The six asymmetric configurations are presented for the Newhall record and each plot has in ordinates the expected value of the square of the displacement at each point of the fourth floor and in the abscissa the plan location in the W(negative)-E(positive) direction. The trends are very clear in the stiffness asymmetric systems. For instance, for configuration S_1, the optimal damper location is quite close to $0.25l_x$; for configuration S_3 instead, the optimal damper location in the weak sense is closer to $e_d = 0.5l_x$. These observations coincide with those obtained from Figures 9 and 10. On the other hand, for the case of mass eccentric systems, none of the configurations is close to satisfy the torsional balance condition $p^* = 0$. Results are consistent with the theory presented since choosing, say, configurations M_2 or M_3, the optimal damper location is closer to $e_d = 0.5l_x$, which is consistent with the standard deviations presented in Figure 10.

Finally, Table 1 provides some additional numerical information regarding the standard deviation of the results of Figures 9 and 10. It also includes normalized rotations and displacements at the CM. In the fifth column, the "type-Ξ" parameter $\Xi = \sigma(\delta_\theta)/\sigma(\delta_{CM}) \times 100$ is included in order to express a quantification of the torsional effect in these six cases. The correlation between lateral and torsional motions is also presented in column 6. The correlation values presented support all conclusions regarding the optimal location of the damper as obtained from Figure 11. Consider for example the S_1 configuration for which the correlation changes sign between $e_d=0.25l_x$ and $e_d=0.5l_x$. This implies that the optimal location of the dampers to achieve weak torsional balance is somewhere in between. The last column of this table contains $H_2 = \sqrt{\sigma^2(\delta_{CM}) + \sigma^2(\delta_\theta)}$ a different norm which enables us to identify the optimal configuration as such with the smallest H_2 value.

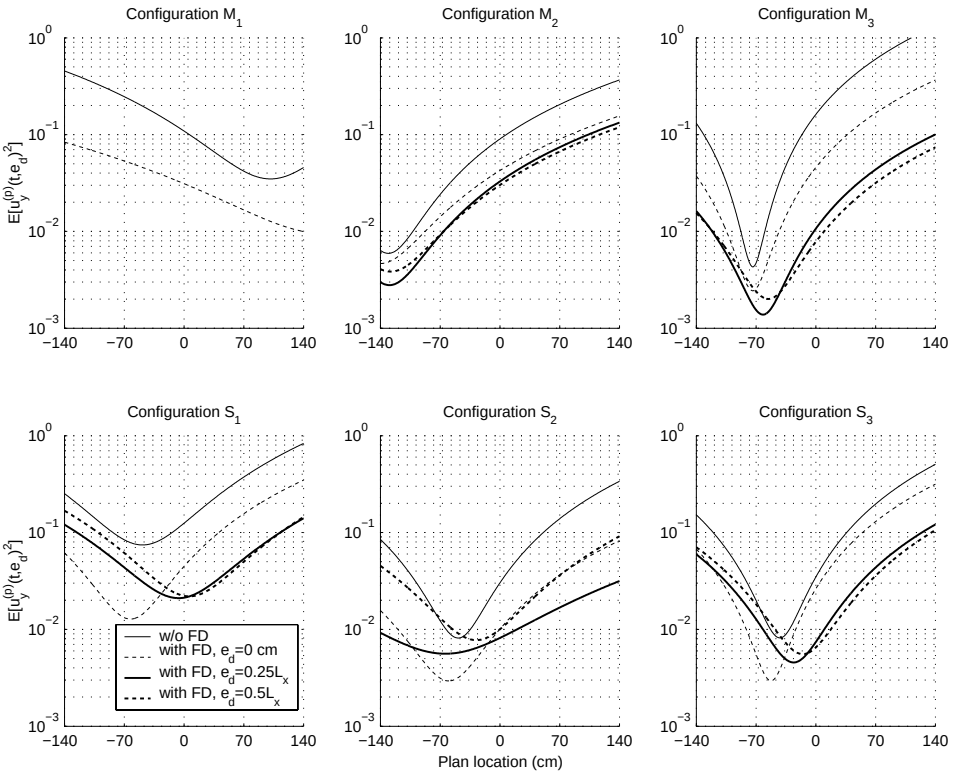

Figure 11. Experimental location of the ECB.

CONCLUSIONS

In this article, the concept of weak torsional balance of single-story elastic structures with frictional and viscoelastic dampers was evaluated analytically and experimentally. The emphasis was placed on the optimal location in plan of the dampers. It was concluded that in addition to the expected reduction in response due to the supplemental damping provided by the dampers, the designer may control the torsional response of the structure by placing the dampers in a position such that the ECB of the structure is at equal distance relative to both edges of the building plan. This weak torsional balance may be extended to control the rotation of the building plan (strong torsional balance) by additional dampers spread apart in the building plan in such a way that the ECB remains coincident with the GC while the radius of gyration of the dampers increase. Because experimental data supports all results that were derived analytically and the concept of the ECB is general, similar trends will be likely obtained in controlling other torsionally unbalanced systems with other type of dampers.

REFERENCES

1. De la llera JC, Chopra AK, Almazán JL. “Three-dimensional inelastic response of an RC during the Northridge Earthquake.” Journal of Structural Engineering, ASCE, 2001; 127 (5): 482-489.
2. De la llera JC, Almazán JL, Vial I. “Torsional balance of plan asymmetric structures with frictional dampers: analytical results.” Earthquake Engineering and Structural Dynamics, 2004. In review (ref: 0345).
3. Vial I. “Torsional balance of plan asymmetric structures with frictional dampers: analytical and experimental results.” Master of Science thesis. Pontificia Universidad Católica de Chile. July 2003.

4. García M. “Balance torsional de estructuras asimétricas utilizando disipadores viscoelásticos.” Master of Science thesis. Pontificia Universidad Católica de Chile. To be submitted May 2004.
5. Lin WH, Chopra AK. “Understanding and predicting effects of supplemental viscous damping on seismic response of asymmetric one-storey systems.” Earthquake Engineering and Structural Dynamics, 2001; 30: 1475-1494.
6. Goel RK. “Effects of supplemental viscous damping on earthquake response of asymmetric-plan systems.” Earthquake Engineering and Structural Dynamics, 1997; 27: 125-141.
7. Pekau OA, Guimond R. “Controlling seismic response of eccentric structures by friction dampers.” Earthquake Engineering and Structural Dynamics, 1991; 20 (6): 505-521.
8. Almazán JL, De la llera JC. “Torsional balance.” Journal of Structural Engineering. To be submitted, 2004.

Table 1. Measured standard deviations of displacements for the scaled Newhall ground motion (20%).

			δ_θ (cm)	δ_{cm} (cm)	δ_{West} (cm)	δ_{East} (cm)	Ξ (%)	$\rho_{\theta x}$	H_2 (cm)
Stiffness eccentric configurations	S_1	w/o FD	0.2203	0.3531	0.2728	0.5216	62.39	-0.6349	0.4162
		with FD, e_d=0	0.1365	0.2115	0.1207	0.3349	64.51	-0.8452	0.2517
		with FD, e_d=0.25L_x	0.1128	0.1458	0.1749	0.1932	77.35	-0.1023	0.1843
		with FD, e_d=0.50L_x	0.1249	0.1490	0.2044	0.1839	83.87	0.1071	0.1944
	S_2	w/o FD	0.1452	0.1738	0.0903	0.3073	83.58	-0.8546	0.2265
		with FD, e_d=0	0.0673	0.1003	0.0568	0.1612	67.10	-0.8417	0.1208
		with FD, e_d=0.25L_x	0.0377	0.0903	0.0760	0.1157	41.79	-0.5588	0.0979
		with FD, e_d=0.50L_x	0.0824	0.1001	0.0946	0.1571	82.29	-0.4765	0.1297
	S_3	w/o FD	0.1851	0.1862	0.0930	0.3595	99.37	-0.8744	0.2625
		with FD, e_d=0	0.1387	0.1619	0.0560	0.2963	85.71	-0.9421	0.2132
		with FD, e_d=0.25L_x	0.0982	0.0861	0.0810	0.1660	114.14	-0.6207	0.1306
		with FD, e_d=0.50L_x	0.0975	0.0807	0.1000	0.1485	120.92	-0.3826	0.1266
Mass eccentric configurations	M_1	w/o FD	0.1283	0.3301	0.4419	0.2357	38.87	0.8247	0.3542
		with FD, e_d=0	0.0426	0.1765	0.2133	0.1429	24.13	0.8342	0.1816
	M_2	w/o FD	0.1060	0.3001	0.1995	0.4036	35.33	-0.9665	0.3183
		with FD, e_d=0	0.0663	0.2063	0.1454	0.2697	32.14	-0.9437	0.2167
		with FD, e_d=0.25L_x	0.0640	0.1811	0.1213	0.2430	35.32	-0.9566	0.1921
		with FD, e_d=0.50L_x	0.0606	0.1736	0.1190	0.2312	34.90	-0.9340	0.1839
	M_3	w/o FD	0.2567	0.4019	0.1544	0.6564	63.87	-0.9866	0.4769
		with FD, e_d=0	0.1348	0.2139	0.0884	0.3464	63.01	-0.9730	0.2528
		with FD, e_d=0.25L_x	0.0744	0.1032	0.0431	0.1747	72.09	-0.9329	0.1272
		with FD, e_d=0.50L_x	0.0655	0.0883	0.0460	0.1485	74.15	-0.8618	0.1099